

IDEA for Restoring Narrow Linewidth of a Gradient-Broadened Magnetic Resonance by Inhomogeneous Dressing

Giuseppe Bevilacqua,¹ Valerio Biancalana,^{1,*} Yordanka Dancheva,² and Antonio Vigilante²

¹*Dept. of Information Engineering and Mathematics - DIISM, University of Siena - Italy*

²*Dept. of Physical Sciences, Earth and Environment - DSFTA, University of Siena - Italy*

(Dated: December 22, 2021)

We study the possibility of counteracting the line-broadening of atomic magnetic resonances due to inhomogeneities of the static magnetic field by means of spatially dependent magnetic dressing driven by an alternating field that oscillates much faster than the Larmor precession frequency. We demonstrate that an intrinsic resonance linewidth of 25 Hz that has been broadened up to hundreds Hz by a magnetic field gradient, can be recovered by the application of appropriate inhomogeneous dressing field. The findings of our experiments may have immediate and important implications, because they facilitate the use of atomic magnetometers as robust, high sensitivity detectors in ultra-low-field NMR imaging.

INTRODUCTION

We propose a method aimed at making optical atomic magnetometers suited to work in an inhomogeneous magnetic field, as those applied for ultra-low-field (ULF) NMR imaging. The method is based on dressing atoms by means of a strong magnetic field that oscillates transversely with respect to the (inhomogeneous) bias field around which they are precessing, at a frequency largely exceeding the local Larmor frequencies.

The magnetic dressing of precessing spins by a harmonic high frequency field has been subject of studies in the late Sixties, when a model was developed based on a quantum mechanical approach [1]. More recently we have re-examined this kind of system in the case of an arbitrary periodic dressing [2], making use of a perturbative approach based on the Magnus expansion [3] of the time-evolution operator.

Magnetic resonance imaging (MRI) at ULF is an emerging method that uses high sensitivity detectors to measure the spatially encoded precession of pre-polarized nuclear spin ensembles in a microTesla-range field [4].

Much like in conventional (high field) MRI, the spatial resolution can be achieved with parallelized measurements based on both frequency and phase encoding: a static inhomogeneity of the main field modulus causes the nuclear spin precess at different frequencies in dependence of one co-ordinate (frequency encoding), while different initial conditions –imposed by pulsed gradients applied prior to the data acquisition– enable a phase encoding, that is used to infer information for the two remaining co-ordinates.

The extremely low precession frequency makes the usual inductive pickup coils disadvantageous detectors at ULF regime, while enables the application of other kinds of detectors, such as superconducting quantum interference devices (SQUIDS) and optical atomic magnetometers (OAMs). These advanced sensors respond adequately to the low frequency signals that characterize the

ULF regime, and may achieve sensitivities at $\text{fT}/\sqrt{\text{Hz}}$ level, making them state-of-the-art magnetometric sensors in MRI as well as in other applications requiring extreme performance.

The feasibility of the ULF-MRI approach has been demonstrated with both kinds of these non-inductive sensors [4, 5]. The ULF MRI is compatible with the presence of other delicate instrumentation, moreover the magnetic detectors can be used to record low-frequency magnetic signals originating from sources other than nuclear spins. In particular, hybrid instrumentation enabling multimodal MRI and MEG measurements has been proposed and implemented [6].

Compared to conventional MRI, the ULF operation brings some relevant advantages. The ultimate spatial resolution of MRI is determined by the NMR linewidth, that in turn depends on the absolute field inhomogeneity. A modest relative homogeneity at ULF turns out to be excellent on the absolute scale: very narrow NMR lines with high signal-to-noise ratio can be recorded at ULF with apparatuses relatively simple in the aspects of the field generation [7–9]. The encoding gradients for ULF MRI can be generated by simple and inexpensive coil systems, as well [10, 11]. Further important advantages of the ULF regime for MRI include the minimization of susceptibility artifacts [12], and possibility of imaging in the presence of conductive materials [8, 13].

The sample-sensor coupling factor is a key feature as in any NMR setup, and in the case of SQUID detectors the need of cryostat may pose limitations. This is an issue that, together with the much lower maintenance cost and the setup robustness, makes the alternative choice of OAM detection attractive.

The OAM detection of NMR signals is based on probing the time evolution of optically pumped atoms that are magnetically coupled to the sample. Differing from other proposed solutions making use of flux transformers [14] and remote detection techniques [15], here we consider the case of atoms precessing in a static field that

is superimposed upon a small term generated by nuclear spins, which are precessing at a much lower rate. In such kind of in-situ MRI setups with OAM detection, the static field gradient applied to the sample for frequency encoding would affect also the atomic precession, with severe degradation of the OAM performance, unless a gradient discontinuity is introduced between the sample and sensor locations, with the need of coil geometries hindering the sample-sensor coupling.

We ideate, test and describe an approach allowing for recording narrow atomic resonances in spite of the presence of an important field inhomogeneity. The proposed method (IDEA, Inhomogeneous Dressing Enhancement of Atomic resonance) is based on counteracting the atomic frequency spread due to a defined field gradient by means of a spatially dependent dressing of the atomic sample. Using this scheme in a MRI setup, the static and the (alternating) dressing fields act inhomogeneously on both the nuclear sample and on the atomic sensor. However, a marked selectivity occurs, because the dressing field effect depends on the gyromagnetic factor, to an extent making the nuclear signal substantially unaffected.

EXPERIMENTAL SETUP

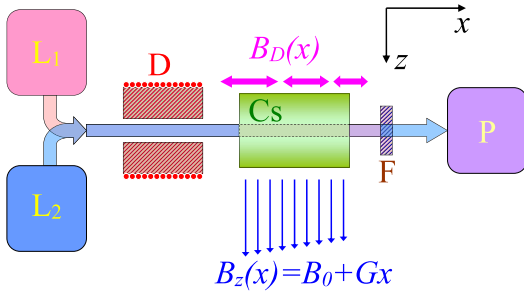


Figure 1. Simplified schematics of the magnetometer and of the fields arrangement (L_1 - pump laser; L_2 probe laser; Cs - Cesium cell; F - interference filter stopping the pump radiation; P - balanced polarimeter). The optical axis of the sensor is x , a static field oriented in z direction has its main component dependent on the x co-ordinate due to a static quadrupolar term producing a gradient $G = \partial B_z / \partial x$. The concomitant $\partial B_x / \partial z$ term has no first order effects on the atomic precession. A dipole D oriented along x produces an oscillating (dressing) magnetic field B_D at a frequency largely exceeding the Larmor frequency. The field B_D is oriented along x and depends on x , as well.

The experimental setup (see Fig.1) is built around an OAM operating in a Bell & Bloom configuration that has been described in detail in Ref.[16].

Briefly, the OAM uses Cs vapor optically pumped into a stretched (maximally oriented) state by means of laser radiation at milli-Watt level. This pump radiation is circularly polarized and tuned to the Cs D_1 line. The

time evolution of the atomic state is probed by a co-propagating weak (micro-Watt level), linearly polarized beam tuned to the proximity of the D_2 line. A transverse magnetic field B_0 causes a precession of the induced magnetization. The magnetization decay is counteracted through synchronous optical pumping, which is obtained by modulating the pump laser wavelength at a frequency $\omega_M/2\pi$ that is resonant with the Larmor frequency $\omega_L/2\pi$. Scanning ω_M around ω_L permits to characterize the resonance profile. In operative conditions, a resonance width of about $\Gamma = 25$ Hz HWHM is measured.

The precession causes a time-dependent Faraday rotation of the probe radiation. This Faraday rotation is driven to oscillate at ω_M (forcing term), to which it responds with a phase $\varphi(t)$ depending on the detuning $\delta = \omega_M - \omega_L = \omega_M - \gamma B$ (γ is the gyromagnetic factor) so to evolve in accordance with the magnetic field B . After the interaction with the vapor, the pump radiation is stopped by an interference filter, and the magnetic field and its variation is extracted from the Faraday rotation of the probe beam measured by a balanced polarimeter. The sensor operates, without any passive shielding, in a homogeneous B_0 field, which is obtained by partially compensating the environmental one, and is oriented along the z axis. B_0 has a typical strength of $4 \mu\text{T}$, giving $T_L = 2\pi/\omega_L \approx 71 \mu\text{s}$.

The atomic vapor (Cs) is contained in a sealed cell with 23 Torr N_2 as a buffer gas, determining a diffusion coefficient $D=3.23 \text{ cm}^2/\text{s}$ [17], that in a precession period causes transverse displacements $\delta = (2DT_L/3)^{1/2} \approx 0.12 \text{ mm}$. The laser beam diameter is $\Phi \approx 1 \text{ cm}$ in diameter, and the condition $\Phi \gg \delta$ enables gradiometric measurements with a base-line of about 5 mm by analyzing the probe spot in two halves [16].

When an inhomogeneous field is applied, the atomic precession in different locations occurs in accordance with the local field, provided that in the motion equation of the atomic magnetization \vec{M}

$$d\vec{M} = - \left(D\nabla^2 \vec{M} + \gamma \vec{B} \times \vec{M} + \Gamma \vec{M} \right) dt \quad (1)$$

the last term in parenthesis exceeds the first one.

This condition sets a limit to the field gradient that can be applied. Requiring that in a precession period T_L the frequency variations due to diffusion in the gradient component $G = \partial B_z / \partial x$ are negligible with respect to Γ results in the condition $G \ll (\sqrt{3}\Gamma)/(\gamma\delta) \approx 1 \mu\text{T}/\text{cm}$, that is largely satisfied.

A well known phenomenon that helps in counteracting the resonance broadening due to field inhomogeneities is the motional narrowing [18, 19]. In cells with very low buffer gas pressure and anti-relaxation coating, both the longitudinal and the transverse relaxation rates decrease proportionally to the buffer gas pressure. In that low-pressure regime, the resonance width increases quadrat-

ically with the gradient, which makes the motional narrowing effective when small gradients are present, while larger gradients cause rapidly increasing widths. For instance, in a 2 cm size evacuated cell, the width is expected (see eq. 62 in Ref.[18]) to exceed our typical Γ for field inhomogeneities above 2 nT/cm.

METHOD

The main goal of this work is to counteract the sensitivity degradation of an OAM using a buffered sensor cell in the high-pressure regime, when placed in a strong linear (quadrupole) magnetic field gradient as that used for MRI frequency encoding [20].

A transverse oscillating field B_D with a inhomogeneity along the x direction is generated by a dipole D oriented along x . Its concomitant gradients produce both transverse (y) and longitudinal (z) oscillating components in the off-axis interaction region. However, these spurious terms have negligible effects.

Fig.1 represents the arrangement for dc (bias, B_z) and ac (dressing, B_D) fields application, the coils for static field and field gradient control are not represented, the schematics of optical part is simplified as well. B_z is oriented along z and its gradient $G = \partial B_z / \partial x$ is set by permanent magnets arranged in a quadrupolar configuration. Thus the Larmor frequency set by B_z is position dependent along the optical axis x .

The dipolar field B_D is produced by an electromagnetic dipole aligned with x : a solenoidal coil is wound on a ferrite nucleus to generate B_D oriented along x with an amplitude decreasing in that direction. The ferrite nucleus has a hollow-cylinder shape, which permits precise alignment without hindering to the propagation of the laser beams.

The dressing field B_D oscillates harmonically and has an axial component

$$B_D(x, t) = \frac{\mu_0}{2\pi} \frac{m(t)}{(x_0 + x)^3} = B_{D0}(x) \cos(\omega t) \quad (2)$$

where μ_0 is the vacuum permittivity, $m(t) = m_0 \cos(\omega t)$ is the oscillating dipole momentum, x_0 is the position of the sensor with respect to the dipole along its axis and x is the displacement from the sensor center. A time dependent current $i(t) = i_0 \cos(\omega t)$ with $\omega \gg \gamma B_z(x) = \Omega(x)$ (γ is the gyromagnetic factor) in the solenoid induces a magnetic dipole with adjustable intensity. The ferrite and the use of resonant circuit help producing a stronger oscillating field (several μ T, in our case).

B_D alters the time evolution of the atomic magnetization in such way to make its x component oscillate harmonically at a dressed (reduced) angular frequency with respect to its unperturbed precession around the static

field [2]:

$$\Omega_D(x) = \Omega(x) J_0(\gamma B_{D0}(x)/\omega), \quad (3)$$

where $J_i(z)$ is the i -th zero-order Bessel function of first kind.

The spatially-dependent dressing can compensate the B_z inhomogeneity at a first order approximation. In fact, being $B_z \approx B_0 + Gx$,

$$\begin{aligned} \Omega_D(x) &= \Omega_D(0) + \Omega'_D(0)x + \frac{1}{2}\Omega''_D(0)x^2 + O(x^3) = \\ &= \gamma B_0 J_0(\alpha) + \gamma [3B_0 \alpha J_1(\alpha) + Gx_0 J_0(\alpha)] \frac{x}{x_0} \\ &\quad - \frac{3\alpha\gamma}{2} [(B_0 - 2Gx_0)J_1(\alpha) + 3\alpha B_0 J_0(\alpha)] \left(\frac{x}{x_0}\right)^2 \\ &\quad + O((x/x_0)^3) \end{aligned}$$

where $\alpha = (\mu_0/2\pi)(\gamma m_0)/(\omega x_0^3)$, and the condition for compensating the gradient G is thus

$$G = -3 \frac{B_0}{x_0} \frac{\alpha J_1(\alpha)}{J_0(\alpha)}, \quad (4)$$

which for values α of experimental interest (up to $\alpha \approx 1$) results in G values up to $1.7(B_0/x_0)$.

In compensated condition (Eq.4), to the second order approximation the angular frequency has the expression

$$\Omega_D(x) \simeq \gamma B_0 \left[J_0 - \beta \left(\frac{x}{x_0} \right)^2 \right] \quad (5)$$

with $\beta = (3\alpha/2J_0)(J_0 J_1 + 6\alpha J_1^2 + 3\alpha J_0^2)$, and $J_i = J_i(\alpha)$.

It is worth noting that β is non-null for any α , meaning that a *Helmholtz condition* (zeroed quadratic term) would require the application of a secondary –weaker– oscillating dipole placed at an opportune, smaller distance on the opposite side of the cell.

RESULTS

We present in Fig.2 a set of spectra obtained in four different conditions, namely in unperturbed conditions, in the presence of a static gradient, in the presence of the same gradient and appropriate dressing compensation, and in the presence of the inhomogeneous dressing having removed the static gradient.

The plot (○) in Fig.2 shows the unperturbed resonance in absence of gradient and dressing field and in optimal operating conditions. At $B_0 = 4 \mu$ T the magnetic resonance amplitude shows a peak at about 14 kHz with a $\Gamma = 25$ Hz line-width HWHM. When quadrupolar magnetic gradient $G = \partial B_z / \partial x = 40$ nT/cm is introduced, the resonance gets broader as shown in the plot (●) in Fig.2.

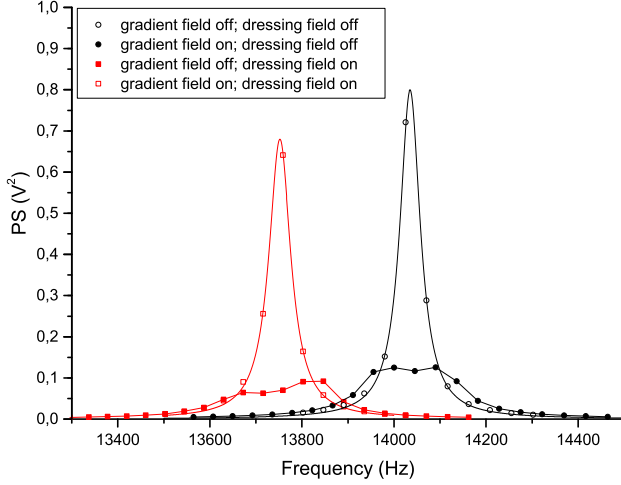


Figure 2. Atomic magnetic resonance in different conditions. The plot (○) shows the unperturbed resonance; (●) in the presence of a static magnetic field gradient; (■) is obtained with no static gradient, but in the presence of a strong, transverse, inhomogeneous field which oscillates much faster than the Larmor precession ($\omega = 2\pi 32$ kHz). This dressing field (amplitude of about $2.4 \mu\text{T}$) produces a resonance shift, that due to its inhomogeneity (600 nT/cm) broadens the resonance. Upon opportune values of amplitude and frequency of the dressing field, the two broadening mechanisms compensate each other, and a shifted but narrow resonance can be recorded, as shown in plot (□).

In the same figure, the plot (■) is obtained in the presence of a strong transverse inhomogeneous field that oscillates much faster than the Larmor precession ($\omega = 2\pi 32$ kHz) and no static gradient. The dressing field B_D has an amplitude of about $2.4 \mu\text{T}$, and shifts the resonance, and –due to the inhomogeneity– broadens it, as well. Under appropriate conditions (eq.4), the two broadening mechanisms compensate each other to the first order, and a shifted but narrow resonance can be recorded, as shown in plot (□). The solid lines are Lorentzian best fits in the cases of narrow resonances (no gradients and dressing-compensated gradient) and eye-guiding interpolations for the two broadened profiles, respectively.

For increasing values of G , the second order term in eq.5 becomes progressively more important, and the dressing optimization cannot restore fully the original linewidths. Fig.3 shows the resonance profiles (under the condition eq.4) for different values of G . For the larger values of G (and consequently stronger dressing), the non-linear term of eq.5 causes a deformation of the resonance profile, with the left wing that slightly exceeds the Lorentzian values. Even for very large G values, the line broadening is effectively compensated, for $G=80 \text{ nT/cm}$ a 34 Hz linewidth (8 Hz broadening) is achieved, to be compared with the 560 Hz that would be observed without the dressing field.

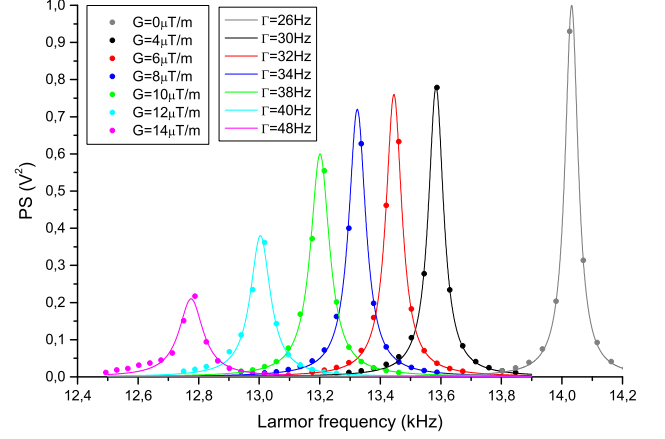


Figure 3. Resonance profile in suppressed-broadening condition, for different levels of G . The dots are measured amplitudes and the lines are best fit targeted to a Lorentzian profile. A progressive shift towards lower frequencies occurs, consistently with eq.3. Simultaneously the profile width increases slightly. Above 100 nT/cm , some deviation from the Lorentzian model due to the higher order terms (Eq.5) appear as an increase in the low-frequency wing. The leftmost plot (recorded at 140 nT/cm) would appear as a 1 kHz broadened resonance in absence of the dressing field.

APPLICATION TO MRI

We have tested the IDEA in a preliminary MRI experiment using remotely polarized protons in tap water, using the setup described in Refs.[21, 22]. Water protons contained in a 4 ml cartridge (pictured in the upper part of Fig.6) are prepolarized in a 1 T field and shuttled to the sensor proximity [23]. The experiment is carried out in unshielded environment, where the environmental magnetic noise is preliminarily reduced by an active stabilization [24] method and then cancelled by measuring differentially on a 5 mm baseline. An automated system permits long-lasting cyclic measurements[21] requiring synchronous control of the shuttling system and video-camera check of its performance, the activation and deactivation of driving field and field-stabilization system, the application of tipping ($\pi/2$) pulses, DAQ and data elaboration.

The dressing factor (Eq.3) for the precessing protons is negligible due to their much lower gyromagnetic factor, so that in the presence of a static gradient their magnetization precesses at a frequency that depends only on the local static field, as in any frequency-encoded MRI experiment. The time-domain recorded signal appears as shown in Fig.4, with and without static gradient, respectively.

Fig.5 shows the effect of static and dressing field inhomogeneities on the spectra of the proton NMR signal. The plot (a) is obtained in a homogeneous static while applying a dressing field. The nuclear signal is insen-

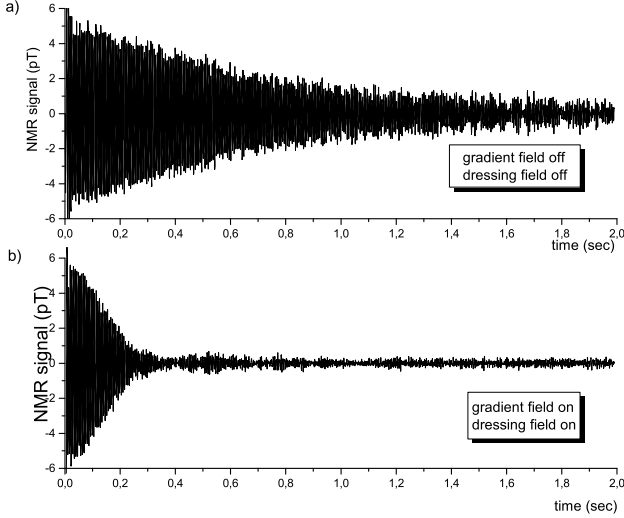


Figure 4. NMR signal from 4ml H₂O sample. The plot a) shows the NMR signal in a homogeneous field, with neither G , nor B_D applied. The trace is obtained by averaging over 100 shots. The plot b) shows the NMR signal recorded in the presence of $G = 50$ nT/cm and $B_D = 3$ μ T. The trace is obtained by averaging over 400 shots.

sitive to B_D while the dressed Cs atoms have position-dependent resonance, so that only a small fraction (slice) are synchronously pumped and contribute effectively in detecting the NMR signal. The recorded resonance has the same width but a worse S/N compared to the case of that resulting for $G = 0$ and $B_D = 0$ (plot b). The application of a static field G broadens both the atomic and the NMR resonances. However (plot c) the whole atomic sensor contributes to a broadened NMR signal detection with a good S/N, thanks to the IDEA method, that restores the atomic resonance linewidth while enabling the registration of position-dependent NMR.

The NMR signal recorded in the presence of the gradient G can be modeled as

$$S(t) = e^{(-\Gamma_N - i\omega_0)t} \int_{-\infty}^{\infty} \eta(x)\rho(x)e^{i\gamma_N G x t} dx \quad (6)$$

where $\eta(x)$ represents the detection efficiency dictated by the sample-sensor coupling and $\rho(x)$ is the proton density in the sample. So, with a standard signal elaboration, after scaling the data by $\exp(\Gamma_N t)$, a Fourier transform reproduces the shape of $\eta(x)\rho(x)$. This is the analysis made on the data corresponding to the plots (b) in Figs. 4 and 5 to reconstruct the $\eta\rho$ profile shown in Fig. 6. An estimate of $\eta(x)$ is made on the basis of the geometry of our experimental setup, and it is used to infer the 1-D image $\rho(x)$ shown in the same figure.

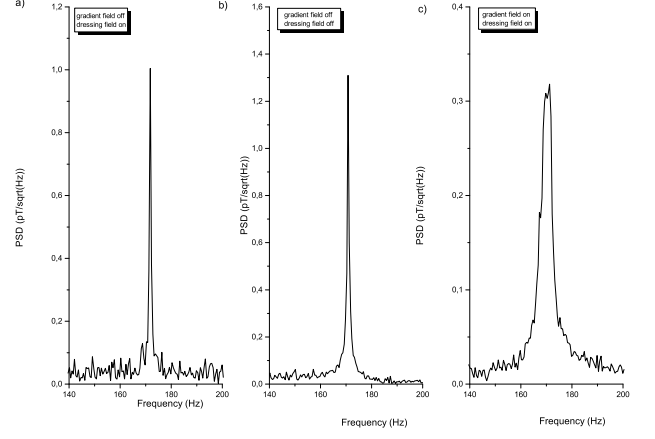


Figure 5. Tap-water proton NMR spectra of the signals in different gradient conditions. The plot a) is obtained with $G = 0$ and $B_D = 3$ μ T: a narrow NMR is recorded, with low S/N, because protons are not affected by B_D , while Cs atoms are, so that only a slice of the sensor is effectively pumped. The plot b) is obtained from the data shown in Fig. 4 a): $G = 0$ and $B_D = 0$ produce narrow NMR with good S/N. The plot c) corresponds to the trace shown in Fig. 4 b), here the static gradient G broadens the NMR spectrum, while the application of IDEA permits to detect it with a good S/N, as the gradient-induced broadening of the atomic resonance is suppressed by the inhomogeneous dressing field B_D .

CONCLUSION

We have proposed, characterized and tested the method IDEA, which –based on magnetically dressing atomic ground-states– enables an atomic magnetometer to operate in the presence of a strong field gradient while preserving its sensitivity, thanks to the suppression of gradient-induced resonance broadening.

We have found accordance between the theoretical model and the observed resonance behavior.

We have provided a preliminary demonstration of the applicability of IDEA to record in the ultra-low-field regime unidimensional NMR images of remotely polarized protons.

Our findings suggest that IDEA constitutes a promising tool for this ULF MRI based on atomic magnetometers. The IDEA method could be applied in shielded volumes and in conjunction with phase-encoding techniques, making several kinds of optical magnetometers suited for being used in 3-D MRI apparatuses, in spite of the important gradients that are necessary to achieve a fine spatial resolution.

ACKNOWLEDGEMENTS

The authors are pleased to thank Alessandra Retico for the useful and interesting discussions.

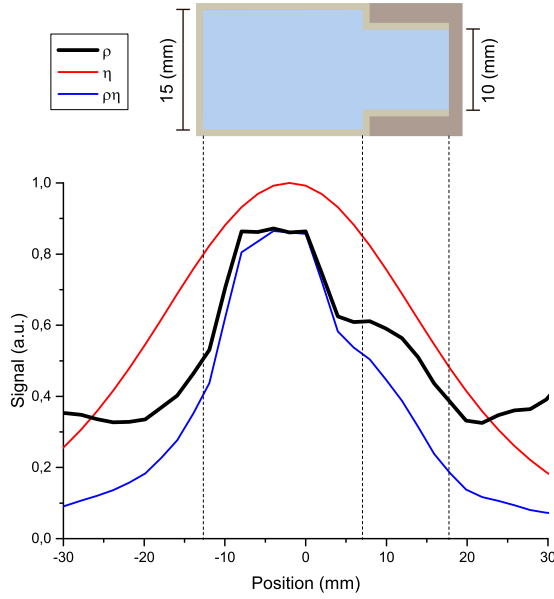


Figure 6. Plots of the measured $\rho(x)\eta(x)$ (blue), the estimated $\eta(x)$ (red) and the inferred $\rho(x)$ (black), which can be compared with the sample shape represented in the upper part. The data are the same shown in the plots b) of Figs.4 and 5. Some position jitter of the sample occurs and is detected shot-by-shot by the camera. To limit the consequent image blurring, only traces corresponding sample positioning within a ± 3 mm interval were selected.

* valerio.biancalana@unisi.it

- [1] S. Haroche, C. Cohen-Tannoudji, C. Audoin, and J. P. Schermann, "Modified Zeeman hyperfine spectra observed in ^1H and ^{87}Rb ground states interacting with a nonresonant RF field," *Phys. Rev. Lett.*, vol. 24, pp. 861–864, 1970.
- [2] G. Bevilacqua, V. Biancalana, Y. Dancheva, and L. Moi, "Larmor frequency dressing by a nonharmonic transverse magnetic field," *Phys. Rev. A*, vol. 85, p. 042510, Apr. 2012.
- [3] W. Magnus, "On the exponential solution of differential equations for a linear operator," *Communications on Pure and Applied Mathematics*, vol. 7, no. 4, pp. 649–673, 1954.
- [4] V. S. Zotev, A. N. Matlachov, P. L. Volegov, A. V. Urbaitis, M. A. Espy, and R. H. K. Jr, "SQUID-based instrumentation for ultralow-field MRI," *Superconductor Science and Technology*, vol. 20, no. 11, p. S367, 2007.
- [5] I. Savukov and T. Karaulanov, "Anatomical MRI with an atomic magnetometer," *Journal of Magnetic Resonance*, vol. 231, pp. 39 – 45, 2013.
- [6] P. T. Vesanen, J. O. Nieminen, K. C. J. Zevenhoven, J. Dabek, L. T. Parkkonen, A. V. Zhdanov, J. Luomaahaara, J. Hassel, J. Penttilä, J. Simola, A. I. Ahonen, J. P. Mäkelä, and R. J. Ilmoniemi, "Hybrid ultra-low-field MRI and magnetoencephalography system based on a commercial whole-head neuromagnetometer," *Magnetic Resonance in Medicine*, vol. 69, no. 6, pp. 1795–1804, 2012.
- [7] R. McDermott, A. H. Trabesinger, M. Mück, E. L. Hahn, A. Pines, and J. Clarke, "Liquid-state NMR and scalar couplings in micro-Tesla magnetic fields," *Science*, vol. 295, no. 5563, pp. 2247–2249, 2002.
- [8] A. N. Matlachov, P. L. Volegov, M. A. Espy, J. S. George, and R. H. Kraus, "SQUID detected NMR in micro-Tesla magnetic fields," *Journal of Magnetic Resonance*, vol. 170, no. 1, pp. 1 – 7, 2004.
- [9] M. Burghoff, S. Hartwig, L. Trahms, and J. Bernarding, "Nuclear magnetic resonance in the nano-Tesla range," *Applied Physics Letters*, vol. 87, no. 5, p. 054103, 2005.
- [10] R. McDermott, S. Lee, B. t. Haken, A. H. Trabesinger, A. Pines, and J. Clarke, "Micro-Tesla MRI with a superconducting quantum interference device," *Proceedings of the National Academy of Sciences*, vol. 101, no. 21, pp. 7857–7861, 2004.
- [11] V. S. Zotev, A. N. Matlachov, P. L. Volegov, H. J. Sandin, M. A. Espy, J. C. Mosher, A. V. Urbaitis, S. G. Newman, and R. H. Kraus, Jr, "Multi-channel SQUID system for MEG and ultra-low-field MRI," *IEEE Trans. Appl. Supercond.*, vol. 17, pp. 839–842, 2007.
- [12] S. K. Lee, M. Mölle, W. Myers, N. Kelso, A. H. Trabesinger, A. Pines, and J. Clarke, "SQUID-detected MRI at 132 μT with T1-weighted contrast established at 10 μT –300 mT," *Magnetic Resonance in Medicine*, vol. 53, no. 1, pp. 9–14, 2004.
- [13] M. Mölle, S.-I. Han, W. R. Myers, S.-K. Lee, N. Kelso, M. Hatridge, A. Pines, and J. Clarke, "SQUID-detected micro-Tesla MRI in the presence of metal," *Journal of Magnetic Resonance*, vol. 179, no. 1, pp. 146 – 151, 2006.
- [14] I. Savukov and T. Karaulanov, "Magnetic-resonance imaging of the human brain with an atomic magnetometer," *Applied Physics Letters*, vol. 103, no. 4, p. 043703, 2013.
- [15] S. Xu, V. V. Yashchuk, M. H. Donaldson, S. M. Rochester, D. Budker, and A. Pines, "Magnetic resonance imaging with an optical atomic magnetometer," *Proceedings of the National Academy of Sciences*, vol. 103, no. 34, pp. 12668–12671, 2006.
- [16] G. Bevilacqua, V. Biancalana, P. Chessa, and Y. Dancheva, "Multichannel optical atomic magnetometer operating in unshielded environment," *Applied Physics B*, vol. 122, no. 4, p. 103, 2016.
- [17] F. A. Franz and C. E. Sooriamoorthi, "Spin relaxation within the $6^2P_{1/2}$ and $6^2S_{1/2}$ states of cesium measured by white-light optical pumping," *Phys. Rev. A*, vol. 10, pp. 126–140, Jul 1974.
- [18] G. D. Cates, S. R. Schaefer, and W. Happer, "Relaxation of spins due to field inhomogeneities in gaseous samples at low magnetic fields and low pressures," *Phys. Rev. A*, vol. 37, pp. 2877–2885, Apr 1988.
- [19] S. Pustelny, D. F. Jackson Kimball, S. M. Rochester, V. V. Yashchuk, and D. Budker, "Influence of magnetic-field inhomogeneity on nonlinear magneto-optical resonances," *Phys. Rev. A*, vol. 74, p. 063406, Dec 2006.
- [20] R. Ansorge and M. Graves, *The Physics and Mathematics of MRI*. 2053-2571, Morgan and Claypool Publishers, 2016.
- [21] G. Bevilacqua, V. Biancalana, Y. Dancheva, A. Vigilante, A. Donati, and C. Rossi, "Simultaneous detection of H and D NMR signals in a micro-Tesla field," *The*

- Journal of Physical Chemistry Letters*, vol. 8, pp. 6176–6179, 2017. PMID: 29211488.
- [22] G. Bevilacqua, V. Biancalana, A. Ben Amar Baranga, Y. Dancheva, and C. Rossi, “Micro-Tesla NMR J-coupling spectroscopy with an unshielded atomic magnetometer,” *Journal of Magnetic Resonance*, vol. 263, pp. 65–70, 2016.
 - [23] Biancalana, Valerio, Dancheva, Yordanka, and Stiaccini, Leonardo, “Note: A fast pneumatic sample-shuttle with attenuated shocks,” *Review of Scientific Instruments*, vol. 85, no. 3, pp. –, 2014.
 - [24] G. Bevilacqua, V. Biancalana, Y. Dancheva, and A. Vigilante, “Machine learning robust control of magnetic disturbances,” *ArXiv*, vol. 1803.03212, 2018.